photolysis) while the atmospheric lifetime is approximately 7 years. The 7-year atmospheric lifetime of $CHF_2Br$ is shorter than the 12- to 18-year lifetime for $CF_2ClBr$ (*7, 11*) and the 65- to 81-year lifetime for $CF_3Br$ (*7, 11*). On a molecule per molecule basis, the improvement obtained by substituting $CHF_2Br$ for $CF_3Br$ is large. The same is not true for replacing $CF_2ClBr$. In the troposphere, $CHF_2Br$ is lost by reaction with OH, unlike $CF_2ClBr$ which is photolyzed. Determinations of lifetimes for species removed by OH reaction are reasonably well established, but tropospheric photolysis loss rates are not as well quantified.


REFERENCES AND NOTES

1. Montreal Protocol on Substances That Deplete the Ozone Layer (United Nations Environmental Programme, New York, 1987).
2. *Chem. Eng. News* **68** (no. 38), 34 (17 September 1990); *Chem. Week.* **146** (no. 21), 35 (30 May 1990).
3. R. S. Sheinson and D. C. Driscoll, paper presented at the 23rd International Symposium on Combustion, Orleans, France, 22–27 July 1990.
4. T. Gierczak, R. Talukdar, G. L. Vaghjiani, E. R. Lovejoy, A. R. Ravishankara, *J. Geophys. Res.* **96**, 5001 (1991).
5. J. B. Burkholder *et al.*, *ibid.*, p. 5025.
6. W. B. DeMore *et al.*, Chemical Kinetics and Photochemical Data for Use in Stratospheric Modeling (Evaluation No. 9, JPL Publication 90-1, Jet Propulsion Laboratory, Pasadena, CA, 1 January 1990).
7. J. J. Orlando, J. B. Burkholder, S. A. McKeen, A. R. Ravishankara, *J. Geophys. Res.* **96**, 5013 (1991).
8. D. A. Fisher *et al.*, *Nature* **344**, 508 (1990).
9. M. Prather and C. M. Spivakovsky, *J. Geophys. Res.* **95**, 18723 (1990).
10. R. G. Prinn and A. Golombek, *Nature* **344**, 47 (1990).
11. Global Ozone Research and Monitoring Project—Report 20, Scientific Assessment of Stratospheric Ozone (World Meteorological Organization, Geneva, 1989), vol. I, p. 430.


12. We thank R. Sheinson for providing the flame suppression data before publication and C. J. Howard for a critical reading of the manuscript. This research was carried out under the Radiatively Important Trace Species (RITS) component of the NOAA Climate and Global Change Program.

11 October 1990; accepted 19 February 1991


# Partial Melting of the Allende (CV3) Meteorite: Implications for Origins of Basaltic Meteorites


A. J. G. JUREWICZ, D. W. MITTLEFEHLDT, J. H. JONES



**Eucrites and angrites are distinct types of basaltic meteorites whose origins are poorly known. Experiments in which samples of the Allende (CV3) carbonaceous chondrite were partially melted indicate that partial melts can resemble either eucrites or angrites, depending only on the oxygen fugacity ($f_{O_2}$). Melts are eucritic if the $f_{O_2}$ is below that of the iron-wüstite buffer or angritic if above the $f_{O_2}$ of that buffer. With changing pressure, the graphite-oxygen redox reaction can produce oxygen fugacities that are above or below those of the iron-wüstite buffer. Therefore, a single, homogeneous, carbonaceous planetoid >110 kilometers in radius could produce melts of drastically different composition, depending on the depth of melting.**


EUCRITES AND ANGRITES ARE DISTINCT classes of basaltic meteorites. The initial Sr isotopic ratios from both groups, which are indistinguishable, indicate great age (*1, 2*). Similarly, their O isotopic compositions suggest derivation from the same isotopic reservoir (*3*), such as planetoids derived from adjacent regions of the solar nebula. Yet there are also radical differences between eucrites and angrites, as indicated by their respective mineralogies. Eucrites are composed mainly of Ca-poor clinopyroxene, anorthitic plagioclase, and tridymite (*4*), whereas angrites contain Ca-, Al-, and Ti-rich clinopyroxene, Ca-rich olivine, and anorthite (*5–7*) (Fig. 1). This difference in mineralogy is a reflection of different bulk compositions. For example, eucrites are silica-saturated, whereas angrites are critically silica-undersaturated. Because of the large difference in the degree of silica saturation between eucrites and angrites, they may be profitably thought of as analogs of terrestrial tholeiites and alkali basalts, respectively. Additionally, the Ca/Al ratios of the most primitive eucrites are close to those of chondritic meteorites, whereas the Ca/Al ratios of angrites are significantly higher (*8*). Eucrites are also thought to have formed under lower ambient oxygen fugacities ($f_{O_2}$) than did the angrites (*9–11*). Accordingly, explanations for the origins of these meteorites must take into account their basaltic textures, distinctive bulk compositions and mineralogies, similar Sr and O isotopic ratios, and different intrinsic $f_{O_2}$.

The origins of eucrites and angrites have been topics of considerable debate. The foci of these debates center around whether these meteorites are evolved melts, produced by complex fractional crystallization processes, or whether they are direct melts from undifferentiated nebular accretions, such as chondritic meteorites. For example, Mason (*12*), and more recently Hewins and Newsom (*13*), viewed eucrites as evolved basaltic liquids. If this hypothesis is correct, an initial, primitive liquid crystallized pyroxene and possibly minor olivine. The evolved, derivative liquid then separated from the accumulation of crystals and was quenched to form eucrites. In contrast, Stolper (*9*) provided evidence that at least some eucrites represent primary, undifferentiated liquids formed by direct melting. Stolper noted that eucrite compositions cluster about a low-pressure peritectic (reaction point) when plotted on a pseudo-ternary olivine-plagioclase-silica (OL-PL-SI) diagram. The compositions of chondritic meteorites can be approximated by this system, and the phase relations imply that peritectic melts of chondrites should be eucritic in composition. Debate over the merits of these end-member models continues.

The origin of angrites is even more obscure. Both complex and simple petrogeneses for angrites have been proposed [for example, (*8*) and references therein]. One suggestion is that angrites may be nebular condensates or slightly modified condensates (*14*). Such diversity of views reflects the strangeness of angrite mineralogies, as contrasted to the mineralogies of other igneous meteorites.

To gain insight into the petrogenesis of eucrites and angrites, we determined experimentally the compositions of low-pressure partial melts of the Allende (CV3) carbonaceous chondrite (*15*) and evaluated the effect of $f_{O_2}$ on melt composition. This meteorite was chosen for pragmatic reasons: representative samples are easily obtained, and the meteorite has been well characterized. Although Allende is not necessarily the best choice for specifically creating melts of either eucritic or angritic bulk composition, its composition (Table 1) was deemed reasonable for an initial assessment of direct melting models (*8*).

Experimental conditions were chosen to reflect inferred conditions of eucrite and angrite genesis. The temperature, 1200°C, was close to both the peritectic temperature of Stolper (*9*) and the liquidus temperature of the angrite LEW86010 (*16*). The $f_{O_2}$ was varied so that the most reducing $f_{O_2}$ was close to that inferred for eucrite genesis (*9*), whereas the higher $f_{O_2}$ values were close to those calculated for LEW86010 (*11*) and measured for Angra dos Reis (*10*). The $f_{O_2}$ values of our experiments bracketed the Fe-FeO (iron-wüstite) O buffer (IW): from one log unit below it (IW−1) to about two


A. J. G. Jurewicz and D. W. Mittlefehldt, Mail Code C23, Lockheed Engineering and Sciences Company, Houston, TX 77058.
J. H. Jones, SN2/Planetary Sciences Branch, National Aeronautics and Space Administration, Johnson Space Center, Houston, TX 77058.

log units above it (IW+2).

For each run, a 125-mg pellet was made from a finely powdered and homogenized sample of Allende (*15*). The pellet was placed on a Pt wire holder and suspended in a Deltech furnace for 4 to 5 days at 1200°C, under flowing $CO/CO_2$ gas which controlled the $f_{O_2}$ (*17*). We analyzed the run products by wavelength-dispersive analysis (*18*), using a Cameca Camebax scanning electron microprobe and standard procedures. Stepwise glass analyses were taken across melt pockets to ensure that analyses were performed as far from crystals as possible. In this way, we tried to avoid analyzing nonrepresentative boundary layers produced during the quench (*19*).

Volatile elements, such as Na, were unavoidably partially lost during the run. However, because we are applying our experiments to basalts that are depleted in volatiles, we anticipated that volatile loss should not affect our conclusions [for example, plagioclase in LEW86010 is essentially end-member anorthite (*6*)]. Comparison of 1- and 5-day experimental glasses at both IW+1 and IW+2 reinforces this view. Although the 1-day charges contained much more $Na_2O$ (>1.4%, by weight), the compositions of the 1- and 5-day glasses were otherwise similar. Apparently, ≤2% $Na_2O$ is insufficient to seriously affect phase relations in our experiments.

Our analyses also indicate that Fe loss to the Pt holder was not significant. In our experimental setup, the sample pellet rests loosely on the Pt. Because the amount of melt is relatively small (~20%, see below), communication between sample and container is poor. Thus, the sample rarely welds to the Pt; and, because we have observed no change in the FeO content of the silicates with experimental duration, we conclude that FeO loss has been minimized.

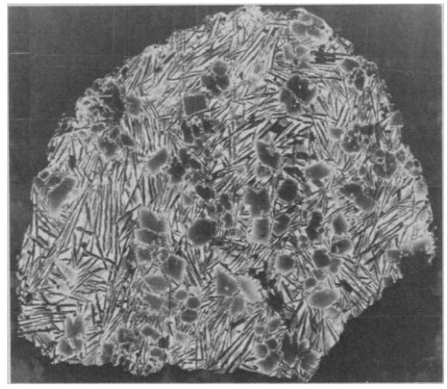

**Fig. 1.** Composite backscattered electron photomicrograph of angrite LEW87051 showing its basaltic igneous texture. This meteorite is one of only three angrites. Backscattered electron imaging maps the mean atomic numbers ($Z$) of phases; brighter areas have higher mean $Z$. Crystals dark in the center and light on the outside are chemically zoned (generally from Mg-rich cores to Fe-rich rims). Zoned, blocky phenocrysts are Ca-rich olivine; the dark elongate crystals are plagioclase that, together with clinopyroxene, makes up most of the groundmass. Section is approximately 5 mm in diameter. [Photo courtesy of NASA and the G. McKay angrite consortium]

The charges were evaluated for chemical equilibrium. Olivine-melt exchange coefficients for Fe and Mg [$K_D$(Fe/Mg)] were in close agreement with those derived from other experiments on angrites [0.28 versus 0.30 in (*16*)] and on eucrites [0.34 versus 0.35 in (*9*)]. Although a few rare, large (~500 μm) original olivines had unequilibrated cores, the melt compositions for major elements were both reproducible and reversible. We performed a reversal experiment by (i) running two charges simultaneously at IW−1, (ii) grinding one charge to less than 74 μm, (iii) pelletizing that charge, and then (iv) running it at IW+2. Analysis of the glasses in both charges agreed with the results of experiments run earlier at IW−1 and IW+2 to within 10% relative. Because the compositions of the IW−1 and IW+2 charges differ by much more than 10% relative, general trends in the data are real. Any minor disequilibrium can be included as part of the experimental uncertainty and does not affect our conclusions.

All charges contained olivine and a spinel phase. Metal was present in some charges, and sulfides were detected in IW−1 charges as inclusions in olivine grains. No other crystalline phases were detected. The Ni, Fe, and Ca contents of olivines increased with increasing $f_{O_2}$: at IW+2, the olivines contained approximately 0.8% CaO by weight, which is consistent with the partitioning systematics determined by Jurewicz and Watson (*20*). Spinel was Cr-rich under reducing conditions but became Al-enriched and more abundant at higher $f_{O_2}$. Metal was Fe-rich at IW−1 (~$Fe_{80}Ni_{20}$) and Ni-rich at IW+1 (~$Fe_{20}Ni_{80}$). No metal was found in contact with glass in the IW+2 charges.

At 1200°C, ~20 ± 5% of the meteorite was molten, irrespective of $f_{O_2}$. The compositions of partial melts formed under reducing conditions were similar to those of eucrites, whereas the compositions of those formed under oxidizing conditions were similar to those of angrites (Table 1 and Fig. 2). The Ca/Al ratios of our glasses increased with increasing $f_{O_2}$. The Ca/Al ratios of melts at IW−1 compare closely to those of eucrites, such as Sioux County; melts at IW+1 and IW+2 have Ca/Al ratios that resemble those of the angrites, LEW86010 and LEW87051. Molar Mg/(Mg+Fe) ratios (Mg#) of the experimental glasses differ significantly from those of the natural meteorites, but this difference may be a function of starting composition as well as $f_{O_2}$. In general, the experimental glasses become increasingly silica-undersaturated with increasing $f_{O_2}$ (Table 2), a pattern consistent with the trend observed in meteorites. The IW−1 glass is hypersthene (Hy)–normative and is nearly quartz (Q)–normative (silica-saturated), whereas the IW+1 and IW+2 glasses are olivine (Ol)- and nepheline (Ne)-normative (critically silica-undersaturated).

Observations suggest that these systematic changes in melt composition with $f_{O_2}$ are caused by changes in the fraction of Fe in

**Table 1.** Composition of meteorites and experimentally produced melts, in percent by weight of oxides. A, Allende (CV3) carbonaceous chondrite starting material (*15*); LEW1, LEW86010; LEW2, LEW87051; ADoR, Angra dos Reis; and SC, Sioux County eucrite. Sioux County is a primitive eucrite whose composition plots close to that of the OL-PL-SI peritectic (Fig. 2B) (*9*). IW−1, IW+1, and IW+2 are melt compositions produced experimentally by partially melting Allende at 1200 °C at an $f_{O_2}$ indicated by the label. Total Fe is reported as FeO. Mg# is defined as molar MgO/(FeO+MgO) × 100, the fraction of (FeO+MgO) that is MgO.

| Oxide | Start, A | Angritic | | | | | Eucritic | |
|---|---|---|---|---|---|---|---|---|
| | | IW+1 | IW+2 | LEW1 | LEW2 | ADoR | IW−1 | SC |
| $SiO_2$ | 34.1 | 39.0 | 38.3 | 39.6 | 40.4 | 43.7 | 47.0 | 49.0 |
| $TiO_2$ | 0.15 | 0.83 | 0.87 | 1.15 | 0.73 | 2.05 | 0.83 | 0.62 |
| $Al_2O_3$ | 3.22 | 13.1 | 12.1 | 14.1 | 9.19 | 9.35 | 13.5 | 12.8 |
| FeO | 30.2 | 23.5 | 22.9 | 18.5 | 19.0 | 9.40 | 19.0 | 18.6 |
| MnO | 0.21 | 0.17 | 0.17 | 0.20 | 0.24 | 0.10 | 0.18 | 0.56 |
| MgO | 24.5 | 5.95 | 5.89 | 7.0 | 19.5 | 10.8 | 7.55 | 7.11 |
| CaO | 2.6 | 15.0 | 15.3 | 17.5 | 10.8 | 22.9 | 12.2 | 10.4 |
| $Na_2O$ | 0.44 | 0.36 | 0.51 | tr | 0.02 | 0.03 | 0.14 | 0.45 |
| $Cr_2O_3$ | 0.54 | 0.05 | 0.04 | 0.11 | 0.17 | 0.21 | 0.28 | 0.35 |
| NiO | 1.62 | 0.09 | 0.16 | | tr | (0.01) | 0.02 | |
| $P_2O_5$ | 0.24 | 0.98 | 1.48 | (0.2) | (0.1) | 0.13 | 0.43 | |
| Total | 97.6 | 99.4 | 97.1 | 98.2 | 99.9 | 98.7 | 99.6 | 100.02 |
| Mg# | 59 | 31 | 32 | 40 | 65 | 67 | 41 | 44 |
| Ca/Al | 1.13 | 1.62 | 1.77 | 1.74 | 1.65 | 3.43 | 1.26 | 1.13 |

the metal phase, as well as by stabilization of aluminous spinel. There is 5 to 10% metal in the IW−1 charge. With increasing $f_{O_2}$, the amount of modal metal decreases and the Ni content of the metal increases. Spinels become increasingly aluminous with increasing $f_{O_2}$. Spinels are small and difficult to analyze. However, our analyses and mass balance calculations for charges run at IW+2 indicate that spinel contains ~45 to 50% $Al_2O_3$ by weight and that only 2 to 3% spinel is enough to account for 30 to 40% of the Al in Allende. Sequestration of this fraction of the Al in Allende is sufficient to raise the Ca/Al ratios of our melts to the values observed at high $f_{O_2}$.

Our results are qualitatively similar to those of Mysen and Kushiro (*21*). These investigators performed low-pressure partial melting of Allende at higher temperatures (1275°C) for the purpose of investigating Ni partitioning between olivine and coexisting melt. Their low $K_D$ values suggest that there was some modification of melt composition during quenching, but the trends in their data are still clear (Fig. 2). The Ca/Al ratio of their experimental glasses increased with increasing $f_{O_2}$, and they pointed out that the stability of aluminous spinels was enhanced.

Our results suggest that partial melting of Allende at low $f_{O_2}$ could form eucritic melts. Thus, bulk Allende satisfies one criterion for the eucrite parent body in that it partially melts at or below ~1200°C, a temperature just above that at which eucrites become fully liquid. Moreover, the partial melt at IW−1 is near the low-pressure peritectic point of Stolper (*9*) (Fig. 2). However, our IW−1 melt is richer in Ca and Al, and somewhat depleted in silica, than natural eucrites. Possibly a bulk composition that is less enriched in refractory lithophile elements such as Ca and Al would be more appropriate for producing eucrites.

Our experiments indicate that, as with eucrites, it is possible to produce angritic liquids from a chondrite directly, as primary partial melts. Thus, angrites need not be formed by extensive fractionations or by nebular condensation. At higher $f_{O_2}$, the FeO content of our melts increases, as does the stability of aluminous spinel. This results in partial melts that are critically silica-undersaturated and that have high Ca/Al ratios. Accordingly, CV chondrites are potential candidates for angrite parent body compositions. However, the need to deplete siderophile elements in angrites (*8*) seems at odds with our inferred redox conditions for angrite genesis (for example, IW+2, where no metal was observed). This apparent inconsistency implies that the angrites may have had a complex redox history, a suggestion supported by the presence of both Fe-metal and titanian magnetite in Angra dos Reis and LEW86010 (*5, 6*).

Could there be a common parent body for the eucrites and angrites? Our results demonstrate that melts ranging in affinity from eucritic to angritic can be generated from a single bulk composition by a simple change in $f_{O_2}$. This observation may indicate that the eucrite parent body was similar in bulk composition to the angrite parent body but had a lower intrinsic $f_{O_2}$. Alternatively, if $f_{O_2}$ varied within an asteroid, it might be possible to generate both eucritic and angritic basalts on the same body. Either a common parent body or a suite of proximal parent bodies could equally account for the similarity in Sr and O isotopic ratios between the eucrites and angrites.

One possible method for producing different $f_{O_2}$ values in a single body is to invoke a pressure-sensitive redox reaction. For example, graphite-CO-$CO_2$ equilibria become increasingly oxidizing as pressure increases (*22, 23*). Moreover, many primitive chondrites contain elemental C (*23*). If reactions involving graphite control the $f_{O_2}$, then $f_{O_2}$ will decrease radially from the center as pressure decreases (*23*). Thus, it seems possible that both eucritic and angritic liquids could form on a single parent body. However, such a body would have to be large enough to produce a pressure differential of at least ~200 bars (*22, 23*). To achieve such pressures requires a minimum radius of ~80 km. For comparison, 4 Vesta, an asteroid believed to be covered by eucrite-like basalts (*24*), is about 250 km in radius.

There is conflicting evidence for formation of angrites in the parent bodies of other meteorite types. If angritic magmas can be brought to the surface from depth by eruptions or by large impacts, then angrite frag-

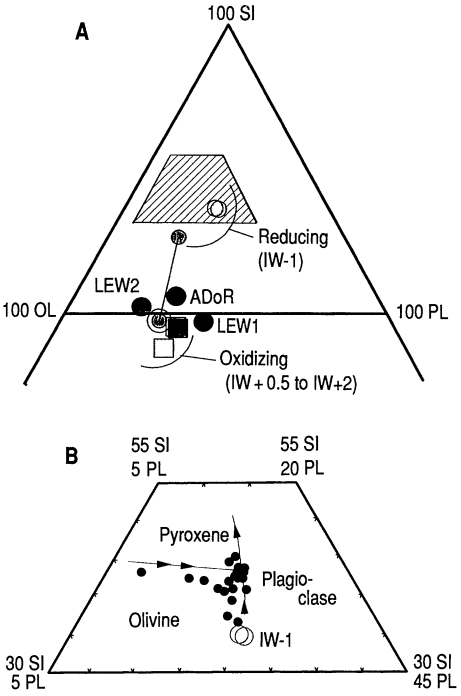


**Fig. 2.** A triangular phase diagram showing the peritectic point in the low-pressure pseudo-ternary system, olivine-plagioclase-silica (OL-PL-SI) [after Stolper (*9*)]. Data are plotted by projection from wollastonite (WO) (*9*). (**A**) The OL-PL-SI diagram of (*9*) with the projection extended to silica undersaturation. Hatchured region is detailed in (B). Experiments from this study (1200°C): open square, IW+2; stippled square, IW−1 remelted at IW+2; open circle, IW−1; stippled circle, IW−1 run with stippled square, but not remelted; filled square, IW+1. Experiments from (*21*) (1275°C): line connects IW−1 (solid end) with superimposed IW+0.5 and IW+2 data points (stippled circle within circle). Filled circles are natural meteorites; the three angrites are labeled, the eucrites are not. The observed displacement of the melt compositions of (*21*) from our own toward OL is what would be predicted at the higher temperatures of (*21*). (**B**) Enlargement of the region around the peritectic point. Filled circles are natural eucrites, others as in (A).

**Table 2.** CIPW norms of meteorites and experimentally produced melts (*28*). Abbreviations: Q, quartz; Or, orthoclase; Ab, albite; An, anorthite; Ne, nepheline; Di, diopside; Hy, hypersthene; Ol, olivine; Cs, dicalcium silicate; Il, ilmenite; Cm, chromite; and Ap, apatite. The norms show similarities and differences in composition, especially silica saturation (low Ol or positive Q) or substantial silica undersaturation (Ne present). The angrites and the melts produced above IW are all Ne-normative. Labels are as in Table 1.

| Mineral | ADoR | LEW1 | LEW2 | IW+1 | IW+2 | SC | IW−1 |
|---|---|---|---|---|---|---|---|
| Q | | | | | | 2.19 | |
| Or | | | | | | | |
| Ab | | | | | | 3.81 | 1.45 |
| An | 25.7 | 39.1 | 25.0 | 34.5 | 30.3 | 33.0 | 38.2 |
| Ne | 0.14 | 0.10 | 0.11 | 1.67 | 2.30 | | |
| Di | 46.0 | 20.9 | 16.5 | 23.4 | 22.0 | 15.5 | 12.0 |
| Hy | | | | | | 43.7 | 43.9 |
| Ol | 13.7 | 29.9 | 54.8 | 34.3 | 37.8 | | 1.62 |
| Cs | 9.86 | 7.28 | 1.83 | 2.20 | 2.29 | | |
| Il | 3.95 | 2.22 | 1.39 | 1.59 | 1.56 | 1.18 | 1.37 |
| Cm | 0.31 | 0.16 | 0.24 | 0.07 | 0.09 | 0.52 | 0.47 |
| Ap | 0.31 | 0.31 | 0.19 | 2.29 | 3.62 | | 1.00 |

ments should be found as clasts in meteorite regolith breccias. Angrite-like material has not been found in the howardites or mesosiderites, which are thought to be surficial breccias of the eucrite parent body. However, angrite-like fragments have been found in polymict ureilites. Polymict ureilites may form the regolith of the ureilite parent body (*25*), thought to be similar in composition to CV or CO carbonaceous chondrites (*26, 27*). If so, it is possible that some basalts on the ureilite parent body are angritic rather than eucritic.

These experimental results indicate that the partial melting of chondritic sources may produce both eucritic and angritic magmas. The differences in major-element compositions between angritic and eucritic magmas are comparable to those between terrestrial tholeiites and alkali basalts. Our experiments show that these differences can be produced without recourse to high-pressure fractionation or volatile fluxing. The production of eucrites by simple partial melting can still be disputed (*13*), but the origin of angritic magmas by a similar mechanism has been hitherto unsuspected.

REFERENCES AND NOTES


1. G. W. Lugmair, S. J. G. Galer, R. Loss, *Lunar Planet. Sci.* **XX**, 604 (1989).
2. L. Nyquist, H. Wiesmann, B. Bansal, C.-Y. Shih, *ibid.*, p. 798.
3. R. N. Clayton and T. K. Mayeda, *Lunar Planet. Inst. Tech. Rep. 90-01* (1990), p. 30.
4. M. B. Duke and L. T. Silver, *Geochim. Cosmochim. Acta* **31**, 401 (1967).
5. M. Prinz *et al.*, *Earth Planet. Sci. Lett.* **35**, 317 (1977).
6. G. A. McKay, D. J. Lindstrom, S.-R. Yang, J. Wagstaff, *Lunar Planet. Sci.* **XIX**, 762 (1988).
7. G. A. McKay, G. Crozaz, J. Wagstaff, S.-R. Yang, L. Lundberg, *ibid.* **XXI**, 771 (1990).
8. D. W. Mittlefehldt and M. M. Lindstrom, *Geochim. Cosmochim. Acta* **54**, 3209 (1990).
9. E. M. Stolper, *ibid.* **41**, 587 (1977).
10. R. Brett, J. S. Huebner, M. Sato, *Earth Planet. Sci. Lett.* **35**, 363 (1977).
11. G. A. McKay, L. Le, J. Wagstaff, *Lunar Planet. Sci.* **XX**, 675 (1989).
12. B. Mason, *Meteorites* (Wiley, New York, 1962).
13. R. H. Hewins and H. E. Newsom, in *Meteorites and the Early Solar System,* J. F. Kerridge and M. S. Matthews, Eds. (Univ. of Arizona Press, Tucson, 1989), pp. 73–101.
14. M. Prinz, M. K. Weisberg, C. E. Nehru, *Lunar Planet. Sci.* **XIX**, 949 (1988).
15. Allende sample 23A-S-1-H-4 was obtained from M. Zolensky, who in turn had received a larger sample from E. King. This sample is characterized in P. Johnson, thesis, University of Houston (1978).
16. G. A. McKay, D. J. Lindstrom, L. Le, S.-R. Yang, *Lunar Planet. Sci.* **XIX**, 760 (1988).
17. R. J. Williams and O. Mullins, Jr., *NASA TMX-58167* (Government Printing Office, Washington, DC, 1976), p. 34.
18. J. I. Goldstein *et al.*, *Practical Scanning Electron Microscopy* (Plenum, New York, 1977).
19. D. A. Kring and G. A. McKay, *Lunar Planet. Sci.* **XV**, 461 (1984).
20. A. J. G. Jurewicz and E. B. Watson, *Contrib. Mineral. Petrol.* **99**, 176 (1988).
21. B. O. Mysen and I. Kushiro, *Carnegie Inst. Washington Yearb.* **75**, 678 (1976).
22. B. M. French and H. P. Eugster, *J. Geophys. Res.* **70**, 1529 (1965).
23. J. H. Berkley and J. H. Jones, *ibid.* **87** (suppl.), A 353 (1982).
24. T. M. McCord, J. B. Adams, T. V. Johnson, *Science* **168**, 1445 (1970).
25. M. Prinz, M. K. Weisberg, C. E. Nehru, J. S. Delaney, *Lunar Planet. Sci.* **XVII**, 681 (1986).
26. J. T. Wasson, C.-L. Chow, R. W. Bild, P. A. Baedecker, *Geochim. Cosmochim. Acta* **40**, 1449 (1976).
27. H. Higuchi *et al.*, *ibid.*, p. 1563.
28. K. C. Cox, J. D. Bell, R. J. Pankhurst, *The Interpretation of Igneous Rocks* (Allen & Unwin, London, 1979).


6 November 1990; accepted 19 February 1991

# Three-Dimensional Structure of Recombinant Human Interferon-γ

STEVEN E. EALICK,* WILLIAM J. COOK, SENADHI VIJAY-KUMAR, MIKE CARSON, TATTANAHALLI L. NAGABHUSHAN, PAUL P. TROTTA, CHARLES E. BUGG

**The x-ray crystal structure of recombinant human interferon-γ has been determined with the use of multiple-isomorphous-replacement techniques. Interferon-γ, which is dimeric in solution, crystallizes with two dimers related by a noncrystallographic twofold axis in the asymmetric unit. The protein is primarily α helical, with six helices in each subunit that comprise ~62 percent of the structure; there is no β sheet. The dimeric structure of human interferon-γ is stabilized by the intertwining of helices across the subunit interface with multiple intersubunit interactions.**

INTERFERON-γ (IFN-γ) IS A PRODUCT of activated T lymphocytes and natural killer (NK) cells that was originally described as an antiviral agent (*1*). IFN-γ exhibits pleiotropic biological activities (*2*) and specifically has been shown to regulate expression of class II major histocompatibility antigens (*3*) and Fc receptors (*4*), activate human monocyte cytotoxicity (*5*), enhance NK cell activity (*6*), and regulate immunoglobulin production and class switching (*7*). Expression of biological activity appears to be mediated through binding to specific cell-surface receptors (*8*), which have been cloned (*9*). The expression of human IFN-γ in *Escherichia coli* (*10, 11*) has resulted in the preparation of large quantities of highly purified recombinant human IFN-γ on which detailed studies of structure-function relations have been initiated (*12–16*).

We reported a preliminary crystallographic study of an *E. coli*–derived recombinant form of human IFN-γ, designated IFN-γ D′, in which the five COOH-terminal residues are deleted (*17, 18*). We report here the determination of the three-dimensional (3-D) structure of recombinant human IFN-γ D′ with the use of multiple isomorphous replacement (MIR) techniques (*19, 20*).

Screening for heavy-atom derivatives was done initially by film methods with synchrotron radiation and subsequently with a Nicolet X-100A area detector (*21*). Eight heavy-atom derivatives were identified, all of which contained multiple sites that made the difference Patterson maps difficult to interpret. Fortunately, one of the derivatives [1 mM $KAu(CN)_2$] contained one site of much higher relative occupancy that could be identified with certainty from the Patterson map. Phases were calculated based on the Au derivative, and the heavy-atom sites of the other derivatives were then located from cross-difference Fourier maps. Heavy-atom parameters were refined with the use of the centric data (Table 1) (*22*); none of the eight derivatives was of high quality. The overall figure-of-merit for data to 3.5 Å resolution for all eight derivatives was 0.74.

Prior to calculation of an electron density map, the phases were improved by solvent-flattening techniques with the ISIR/ISAS package of programs by Wang (*23*). The initial molecular envelope was determined by assuming a solvent fraction of 50%. After convergence, the overall figure-of-merit was 0.85, the average accumulated phase shift was 21°, the $R$ factor between calculated structure factors ($F_c$) after map inversion and observed structure factors ($F_o$) was 0.282, and the correlation coefficient between $F_o$ and $F_c$ was 0.95. The electron density map calculated with these phases

S. E. Ealick, Department of Pharmacology, Center for Macromolecular Crystallography and Comprehensive Cancer Center, University of Alabama at Birmingham, Birmingham, AL 35294.
W. J. Cook, Department of Pathology, Center for Macromolecular Crystallography and Comprehensive Cancer Center, University of Alabama at Birmingham, Birmingham, AL 35294.
S. Vijay-Kumar and M. Carson, Center for Macromolecular Crystallography, University of Alabama at Birmingham, Birmingham, AL 35294.
T. L. Nagabhushan and P. P. Trotta, Schering-Plough Research, Bloomfield, NJ 07003.
C. E. Bugg, Department of Biochemistry, Center for Macromolecular Crystallography and Comprehensive Cancer Center, University of Alabama at Birmingham, Birmingham, AL 35294.

*To whom correspondence should be addressed.